Theoretical Implementation of All-Optical XOR Gate at 160 Gb/s Using Semiconductor Optical Amplifiers-Based Turbo-Switched Mach-Zehnder Interferometer

Amer Kotb,[a,b,*] Chunlei Guo[a,c,*]
[a]The Guo China-US Photonics Laboratory, Changchun Institute of Optics, Fine Mechanics, and Physics, Chinese Academy of Sciences, Changchun 130033, China
[b]Department of Physics, Faculty of Science, University of Fayoum, Fayoum 63514, Egypt
[c]The Institute of Optics, University of Rochester, Rochester, NY 14627, USA

Abstract: The implantation of an all-optical eXclusive-OR (XOR) gate run at 160 Gb/s using semiconductor optical amplifiers (SOAs)-based turbo-switched Mach-Zehnder interferometer (TS-MZI) is theoretically investigated and verified. The dependence of the quality factor (QF) on the signal and SOA key operating parameters is examined and assessed, including the impact of amplified spontaneous emission in order to obtain realistic results. A higher QF is obtained when using SOAs-based TS-MZI than when using conventional SOAs-based MZI.

Keywords: all-optical XOR gate, semiconductor optical amplifier, turbo-switched Mach-Zehnder interferometer.

***** Correspondence Authors**,** E-mails: amer@ciomp.ac.cn (Amer Kotb); guo@optics.rochester.edu (Chunlei Guo)

1 Introduction

The continuous searching for low-cost all-optical logic gates (AOLGs) with high-capacity information has been developed. On the other hand, a semiconductor optical amplifier (SOA) plays an important role as a nonlinear element in communication systems due to its high-nonlinearity, low-cost, stability, low-power consumption, small size, and compactness. The performance of all-optical exclusive-OR (XOR) operation using SOA-based Mach-Zehnder interferometer (MZI) has been designed and modeled[1-16]. Practically, those schemes have been successfully developed by employing an integrated MZI due to its high stability, low-energy requirement, simplicity, and compactness. However, the speed of the SOA does not exceed ~ 100 Gb/s due to its slow carrier recovery time response, which results in pattern-dependent dynamic behavior and performance degradation at higher bit rates[17]. Therefore, it's important to confront this problem by speeding up its carrier recovery time

to meet the need for the high-speed communication systems. Multi-designs have been reported to overcome the limitation of the SOA[18-22], but most of these designs are difficult to integrate into the real systems[19-21] and some cause heat generation or instability of SOA[20,22]. To confront this problem, the turbo-switched (TS) MZI, where an extra pair of SOA is cascaded and separated by broadband optical filters (OFs), is used to overcome the limitation of the SOA carrier dynamics. The extra SOAs act as nonlinear filters to compensate for the slow recovery component of the signal emerging from the first SOA, thus shortening the overall recovery time response of the whole SOAs combination over the single SOA. It would be beneficial to further implement the all-optical operations with an acceptable performance when using SOAs-based TS-MZI than standard SOAs-based MZI. Thus, in this paper, we compare, by means of the numerical analysis, between the performance of the all-optical XOR gate using SOAs-based TS-MZI and conventional SOAs-based MZI at 160 Gb/s. The variation of the gate quality factor (QF) against the signal and SOA operating parameters, which include the pulse energy and width, data rate, equivalent length of pseudorandom bit sequence (PRBS), length and thickness of SOA active region, confinement factor, traditional linewidth enhancement factor (α-factor), injection current, saturation power, carrier lifetime, and amplified spontaneous emission (ASE) has been examined and assessed. The results obtained through this study demonstrate indeed the feasibility of using the SOAs-based TS-MZI scheme to execute the XOR gate at 160 Gb/s with better performance than the standard SOA-based MZI.

The rest of this paper is organized as follows: The operation principle and the numerical analysis of the XOR implementation are formulated in Section 2. The results of the XOR gate is presented in Section 3. Finally, Section 4 contains the concluding remarks.

2 XOR implementation

2.1 Operation principle

The schematic structure and truth table for the all-optical XOR operation using SOAs-based TS-MZI are shown in Fig. 1.

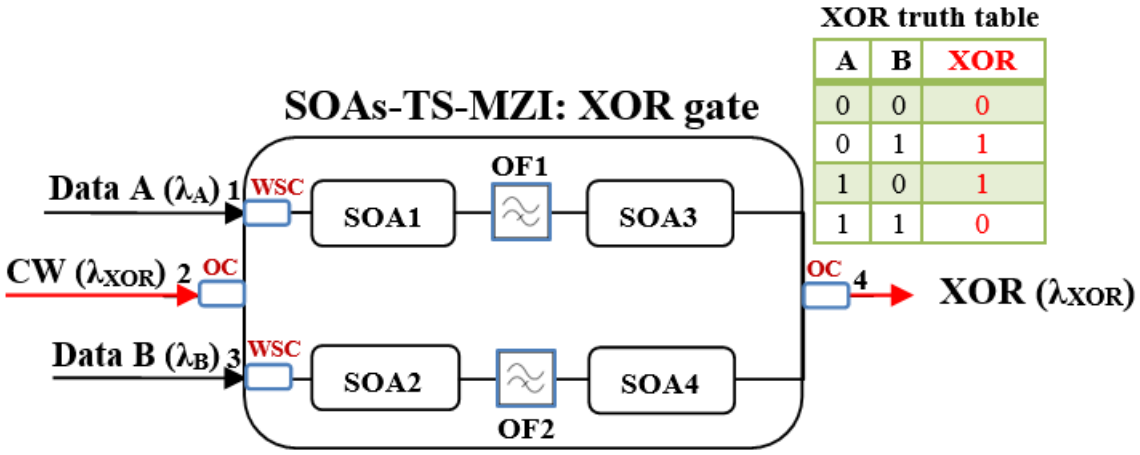

XOR truth table

A	B	XOR
0	0	0
0	1	1
1	0	1
1	1	0

Fig. 1. Schematic diagram and truth table of all-optical XOR gate using SOAs-based TS-MZI. OC: 3 dB Optical Coupler. WSC: Wavelength Selective Coupler. OF: Optical Filter.

In order to realize the XOR operation, a CW probe signal at a wavelength λ_{XOR}, which is the assigned output signal wavelength, is equally split via the 3 dB optical coupler and injected from port 2 into the middle arm of the SOAs-TS-MZI. The CW half is combined with data signal A at a wavelength of λ_A via the wavelength selective coupler (WSC) and inserted from port 1, while the other CW half is combined with data signal B at λ_B via WSC and inserted from port 3. λ_{XOR} must be different from λ_A and λ_B, which they are not necessary to be different. The input signals A and B are Gaussian-shaped pulses with two different pseudo-random bit sequence (PRBS). Data A and B modify the phase of the CW probe beam via cross-phase modulation in the SOAs. When both A and B are logically the same, '0' or '1', no phase on CW is formed and the output is null. A phase induced on CW only when A and B are different logic input. In this case, the CW interfere constructively and the output is '1'. In this manner, the XOR operation is executed according to its truth table.

2.2 Numerical analysis

In this study, all SOAs are assumed to be identical. The process of the carrier's transition from the conduction band to the valence band is known as the carrier-depletion (CD). The other nonlinear effects contribute to the gain process are the carrier-heating (CH), which occurs between 0.1 ps – 0.7 ps and results from carriers' thermalization in the entire energy band following the pulse, and spectral-hole burning (SHB), which results from burning a hole in the gain spectrum. These nonlinear effects included CD, CH, and SHB are taken into account to describe the time-dependent gain of each SOA by the following first-order differential equations[23,24]:

$$\frac{dh_{CD}(t)}{dt} = \frac{h_0 - h_{CD}(t)}{\tau_C} - (exp[h_{CD}(t) + h_{CH}(t) + h_{SHB}(t)] - 1)(P_{in}(t)/E_{sat}) \quad (1)$$

$$\frac{dh_{CH}(t)}{dt} = -\frac{h_{CH}(t)}{\tau_{CH}} - \frac{\varepsilon_{CH}}{\tau_{CH}}(exp[h_{CD}(t) + h_{CH}(t) + h_{SHB}(t)] - 1)\, P_{in}(t) \quad (2)$$

$$\frac{dh_{SHB}(t)}{dt} = -\frac{h_{SHB}(t)}{\tau_{SHB}} - \frac{\varepsilon_{SHB}}{\tau_{SHB}}(exp[h_{CD}(t) + h_{CH}(t) + h_{SHB}(t)] - 1)\, P_{in}(t) - \frac{dh_{CD}(t)}{dt} - \frac{dh_{CH}(t)}{dt} \quad (3)$$

where functions 'h' represent the SOA gain over its length due to the dynamic processes of CD, CH, and SHB. $h_0 = \mathrm{Log}[G_0]$, where G_0 is the unsaturated power gain. $P_{in}(t)$ is the input signal power, which is linked to the light intensity (S(t)) via $P(t) = \kappa\, S(t)$, where κ is the conversion factor. E_{sat} is the saturation energy, which is related to the saturation power (P_{sat}) via $E_{sat} = P_{sat}\,\tau_c$, where τ_c is the carrier lifetime. The temperature relaxation and the carrier-carrier scattering rates are τ_{CH} and τ_{SHB}, respectively. ε_{CH} and ε_{SHB} are the nonlinear gain suppression factors of CH and SHB, respectively.

The total output gain (G(t)) of each SOA is given by:

$$G(t) = exp[h_{CD}(t) + h_{CH}(t) + h_{SHB}(t)] \quad (4)$$

While the phase change of each SOA is given by:

$$\Phi(t) = -0.5(\alpha\, h_{CD}(t) + \alpha_{CH}\, h_{CH}(t) + \alpha_{SHB}\, h_{SHB}(t)) \quad (5)$$

where α is the traditional linewidth enhancement factor (α-factor), α_{CH} and α_{SHB} are the linewidth enhancement factors due to CH and SHB, respectively. Because the SHB produces a nearly symmetrical spectral hole centered at the signal wavelength, the value of α_{SHB} is null[25].

The input power of signals A and B are assumed to be Gaussian-shaped pulses, i.e.,

$$P_{A,B}(t) \equiv P_{in}(t) = \sum_{n=1}^{N} a_{nA,B} \frac{2\sqrt{\ln(2)}\,E_0}{\sqrt{\pi}\,\tau_{FWHM}} \exp\left[-\frac{4\ln(2)(t-nT)^2}{\tau_{FWHM}^2}\right] \tag{6}$$

where $\alpha_{nA,B}$ is the n-th pulse of logical '1' or '0' with equal probability inside a PRBS of length 2^7-1 that contains pulses having the energy (E_0), full-width at half maximum (FWHM) pulse width (τ_{FWHM}), and bit period (T). The input signal powers injected into the upper and the lower arms of the SOAs-TS-MZI are, respectively, described by the following equations:

$$P_{in1}(t) = P_A(t) + 0.5P_{CW} \tag{7}$$

$$P_{in2}(t) = 0.5P_{CW} + P_B(t) \tag{8}$$

where the coefficient '0.5' takes into account the coupling of CW beam into the two arms of SOAs-TS-MZI.

In this simulation, the optical filter (OF) is considered to be a Gaussian-shaped whose filed transfer function in the frequency domain is described as[26]:

$$OF_{1,2}(f) = \exp\left[-Log[\sqrt{2}]\left(\frac{f - f_c}{B/2}\right)^{2N}\right] \tag{9}$$

where f is the frequency of the input signal, f_c is the center frequency of the filter, B is the optical bandwidth of the filter, and N is order of the filter, which determines the sharpness of its passband edges, where $N = 1$ corresponds to Gaussian and $N \geq 2$ to super-Gaussian shapes[26].

The electric field emerging from SOA1 and SOA2 is calculated by applying the amplitude gain (G(t)) and the phase (Φ(t)) to the input electric filed, i.e.,[27]:

$$E_{out,SOA_{1,2}}(t) = \sqrt{0.5P_{CW}}\,\exp\left[-0.5\,Log\left[G_{SOA_{1,2}}(t)\right] + j\,\Phi_{SOA_{1,2}}(t)\right] \tag{10}$$

The power inserted into SOA3 and SOA4 is that of the signals coming out of OF1 and OF2, respectively, which is analogous to the square modulus of the corresponding electric field, $E_{OF_{1,2}}(t)$ [27]:

$$P_{in,SOA_{3,4}} \equiv P_{OF_{1,2}}(t) = \left|E_{OF_{1,2}}(t)\right|^2 = \left|F^{-1}\left\{F\left[E_{out,SOA_{1,2}}(t)\right]\cdot OF_{1,2}[f]\right\}\right|^2 \tag{11}$$

where operators $F[\cdot]$ and $F^{-1}[\cdot]$ denote the Fourier transform and its inverse, respectively.

The output electric field coming from SOA3 and SOA4 is described as[27]:

$$E_{out,\,SOA_{3,4}}(t) = E_{OF_{1,2}}(t)\cdot\exp\left\{0.5\ln[G_{SOA_{3,4}}(t)] + j\,\Phi_{SOA_{3,4}}(t)\right\} \tag{12}$$

Using the mathematical formulations for the operation of the SOAs-TS-MZI, the output XOR power is given by:

$$P_{\text{out, XOR}}(t) = \left[\left|E_{SOA_3}(t)\right|^2 + \left|E_{SOA_4}(t)\right|^2\right] \Big/ 2 \tag{13}$$

3 XOR Results

The metric used in this paper to evaluate the performance of the considered Boolean functions is the QF, which is defined as QF = $(P_1 - P_0) / (\sigma_1 + \sigma_0)$[23], where $P_{1,0}$ are the mean peak powers of the logic '1's & '0's and $\sigma_{1,0}$ are the corresponding standard deviations. The QF and the bit-error-rate (BER)[28] are linked through $BER = 0.5\ erfc[QF/\sqrt{2}] \approx \exp[-QF^2/2]/QF\sqrt{2\pi}$, where erfc is the error function. The acceptable QF must more than 6 to ensure that the BER is less than 10^{-9}, which is acceptable for the digital logic[23]. The symbol, definition, value, and unit of the key parameters used in this study are cited in Table 1[23-29].

Table 1 Calculation parameters.

Symbol	Definition	Value	Unit
E_0	Pulse energy	0.08	pJ
τ_{FWHM}	Pulse width	0.5	ps
n	PRBS length	127	-
T	Bit period	6.25	ps
L	Length of active region	0.5	mm
d	Thickness of active region	0.2	μm
I	Injection current	200	mA
Γ	Confinement factor	0.3	-
τ_c	Carrier lifetime	100	ps
α	α-factor	8	-
α_{CH}	Linewidth enhancement factor due to CH	1	-
α_{SHB}	SHB α-factor	0	-
τ_{CH}	Temperature relaxation rate	0.3	ps
τ_{SHB}	Carrier-carrier scattering rate	0.1	ps
ε_{CH}	CH nonlinear gain suppression factor	0.02	W^{-1}
ε_{SHB}	SHB nonlinear gain suppression factor	0.02	W^{-1}
G_0	Unsaturated power gain	30	dB
P_{sat}	Saturation power	35	mW
f_A	Frequency of data A	189.7	THz
f_B	Frequency of data B	189.7	THz
f_{CW}	Frequency of CW probe	194.7	THz
f_c	Center frequency of filter	194.7	THz
P_A	Power of data A	1	mW
P_B	Power of data B	1	mW
P_{CW}	Power of CW probe	2	mW
B	Optical bandwidth of filter	3	nm
N	Order of filter	2	-
N_{sp}	Spontaneous emission factor	2	-
B_0	Optical bandwidth	2	nm

To evaluate the advantages of the TS-MZI, Figs. 2 and 3 show the numerical results and eye diagrams for the XOR gate at 160 Gb/s using the SOAs-based TS-MZI and standard SOAs-based MZI, respectively. The obtained QFs are 23 using SOAs-based TS-MZI and 11 using SOAs-based MZI. This can be ascribed to a higher amplifier nonlinear response caused by the SOAs-based TS-MZI. The values of the BER are also displayed for each eye diagram. Practically, the TS-MZI can be considered as an error-free[29].

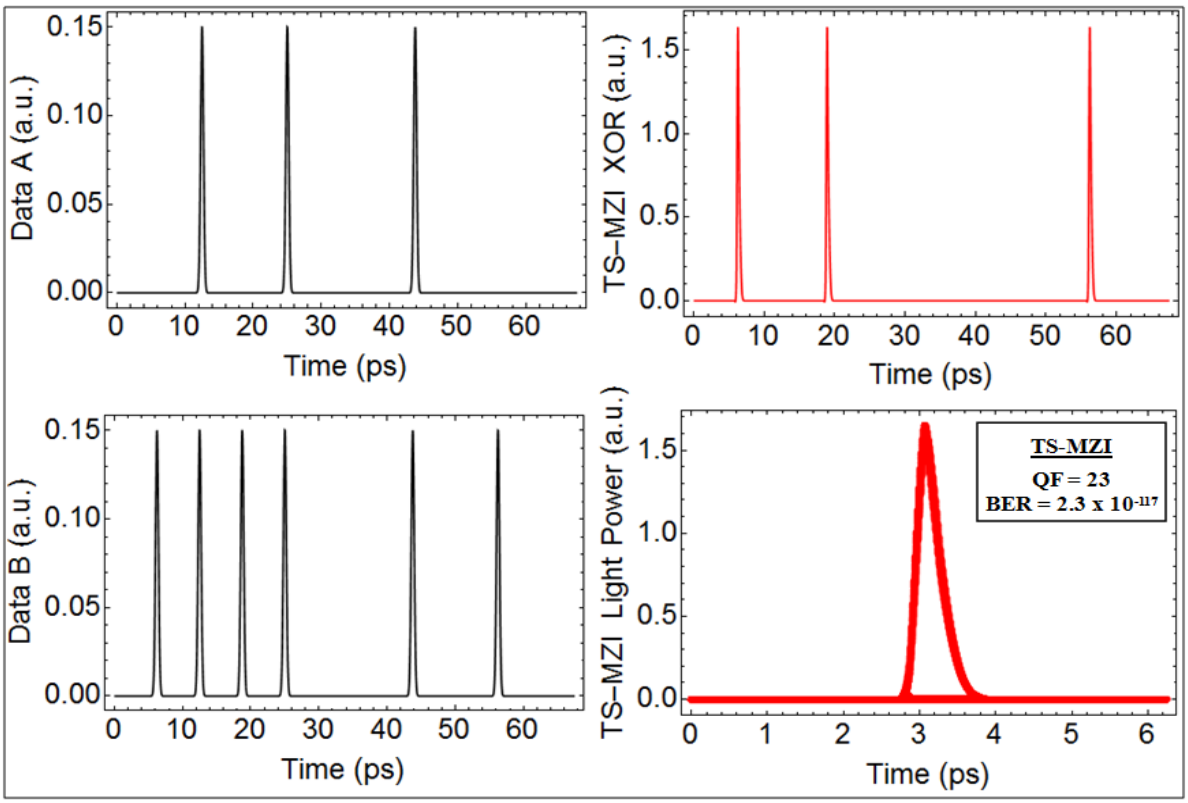

Fig. 2. Numerical results and eye diagram for XOR operation using SOAs-based TS-MZI at 160 Gb/s.

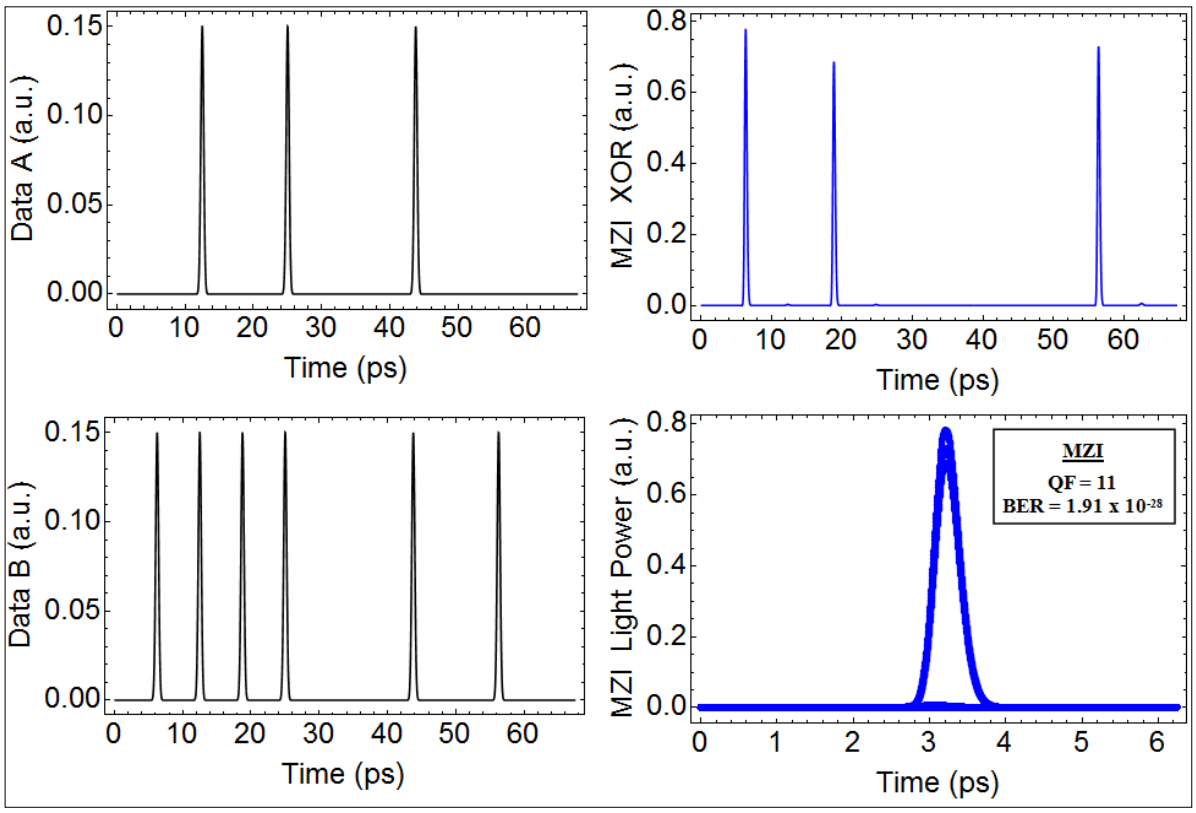

Fig. 3. Numerical results and eye diagram for XOR operation using SOAs-based MZI at 160 Gb/s.

The main purpose of the OFs is to block the modulated pump beams that cross the originality CW beam in SOA1 and SOA2. The SOA3 and SOA4 play an important role in the acceleration of the overall nonlinear dynamical processes, which decrease the data-pattern effects. In order to investigate the role of the OFs adjusted before the two extra SOAs, Fig. 4 shows the output powers of SOA1 and SOA2 before and after entering the OFs.

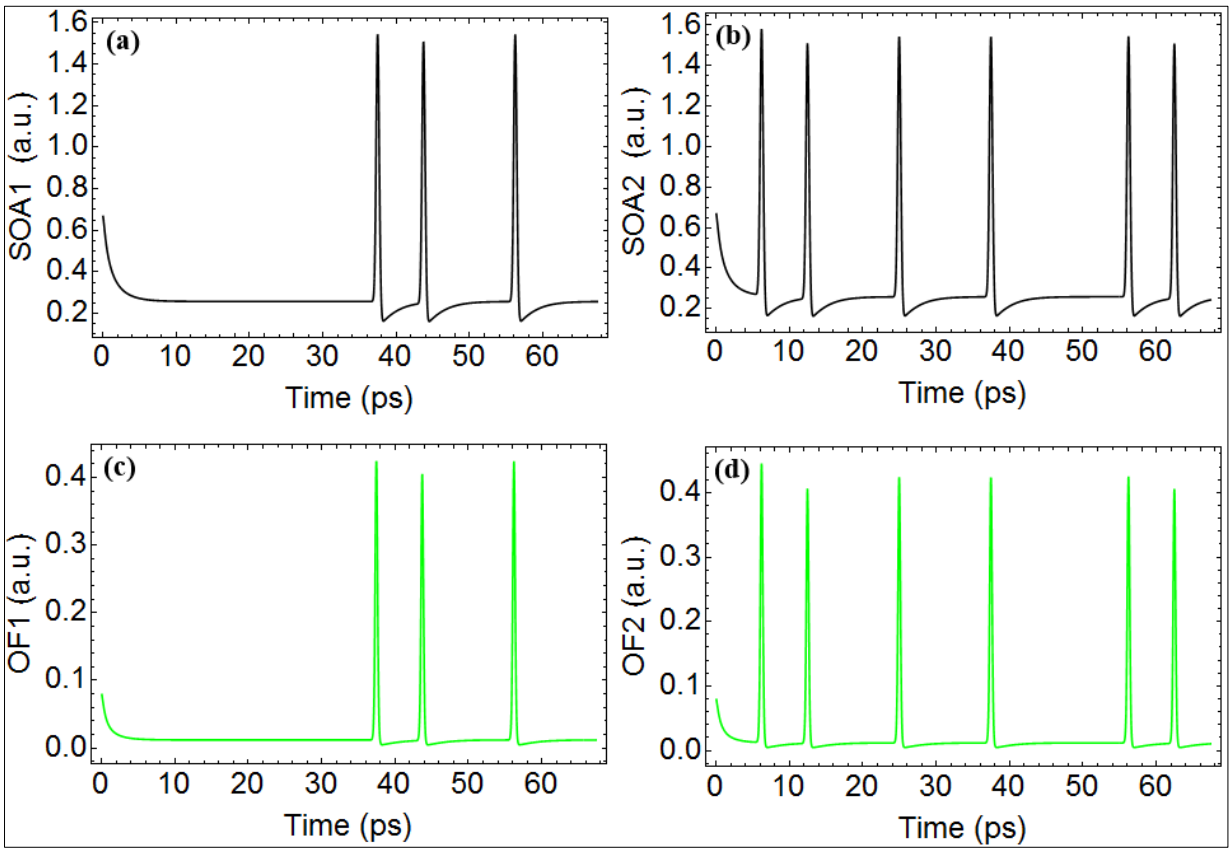

Fig. 4. Numerical results (a), (b) before and (c) and (d) after the optical filters.

The variation of the XOR QF against the input signal key parameters, including the energy, width, data rate, and equivalent length of PRBS using the SOAs-TS-MZI and standard SOAs-MZI at 160 Gb/s is shown in Fig. 5(a)-(d). Generally, as the input pulses become more energetic and broader, the QF is decreased as shown in Fig. 5(a) and (b) due to the heavy gain saturation of the SOAs. A similar observation is shown in Fig. 5(c), where the QF is dropped with increasing the data rate. Because of the ultrafast speed response of SOA caused when using the TS-MZI, the pattern effects are almost absent. For this reason, the AOLGs based on the SOAs-TS-MZI can be worked at high data rates with

more acceptable performances than the typical SOAs-MZI. In fact, the performance of the XOR operation isn't affected by the BRBS higher lengths and remains an acceptable for both SOAs-based TS-MZI and SOAs-based MZI as shown in Fig. 5(d).

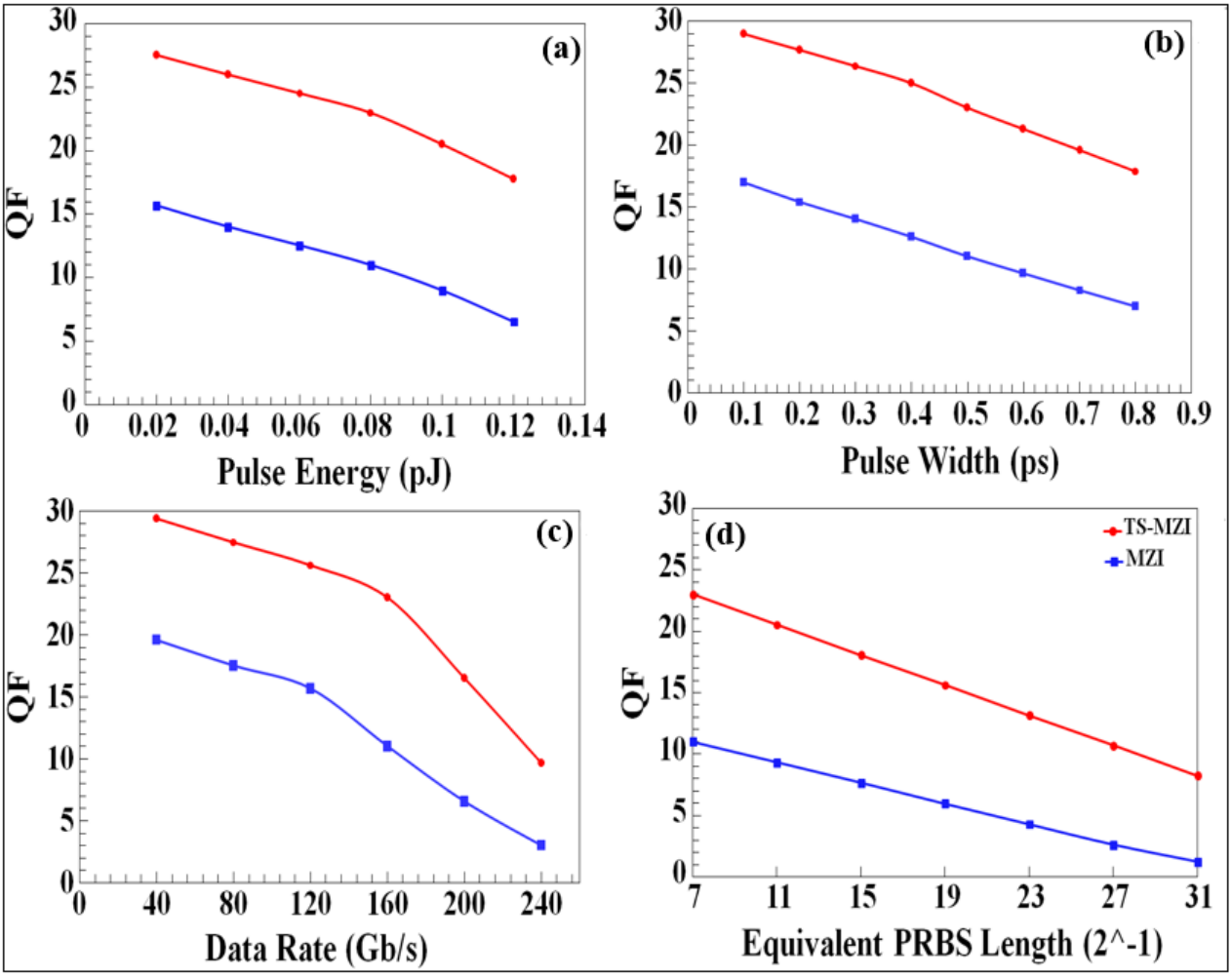

Fig. 5. QF vs. (a) pulse energy, (b) pulse width, (c) data rate, and (d) equivalent length of PRBS using SOAs-based TS-MZI and SOAs-based MZI for XOR operation at 160 Gb/s.

In this part, we discuss the dependence of the QF on the SOA operating parameters, including the length and thickness of the SOA active region, confinement factor, and α-factor for both schemes, TS-MZI and MZI-based XOR operation at 160 Gb/s. The QF is increased for longer and thicker active regions as shown in Fig. 6(a) and (b), respectively. The QF using the SOAs-based TS-MZI is still more acceptable even for a higher SOA size than when using standard SOAs-based MZI. This difference is attributed to the optical filters, which reduces the pattern effects and hence increases the optical gain

during the whole size of SOAs-TS-MZI. Similar observations are seen in Fig. 6(c) and (d) where the QF against the confinement factor (Γ) and α-factor. At low values of Γ and α-factor, the output signal is degraded and the QF is decreased. Actually, using a higher α-factor provides an acceptable performance since it creates the necessary level of differential phase shift required in the switching module.

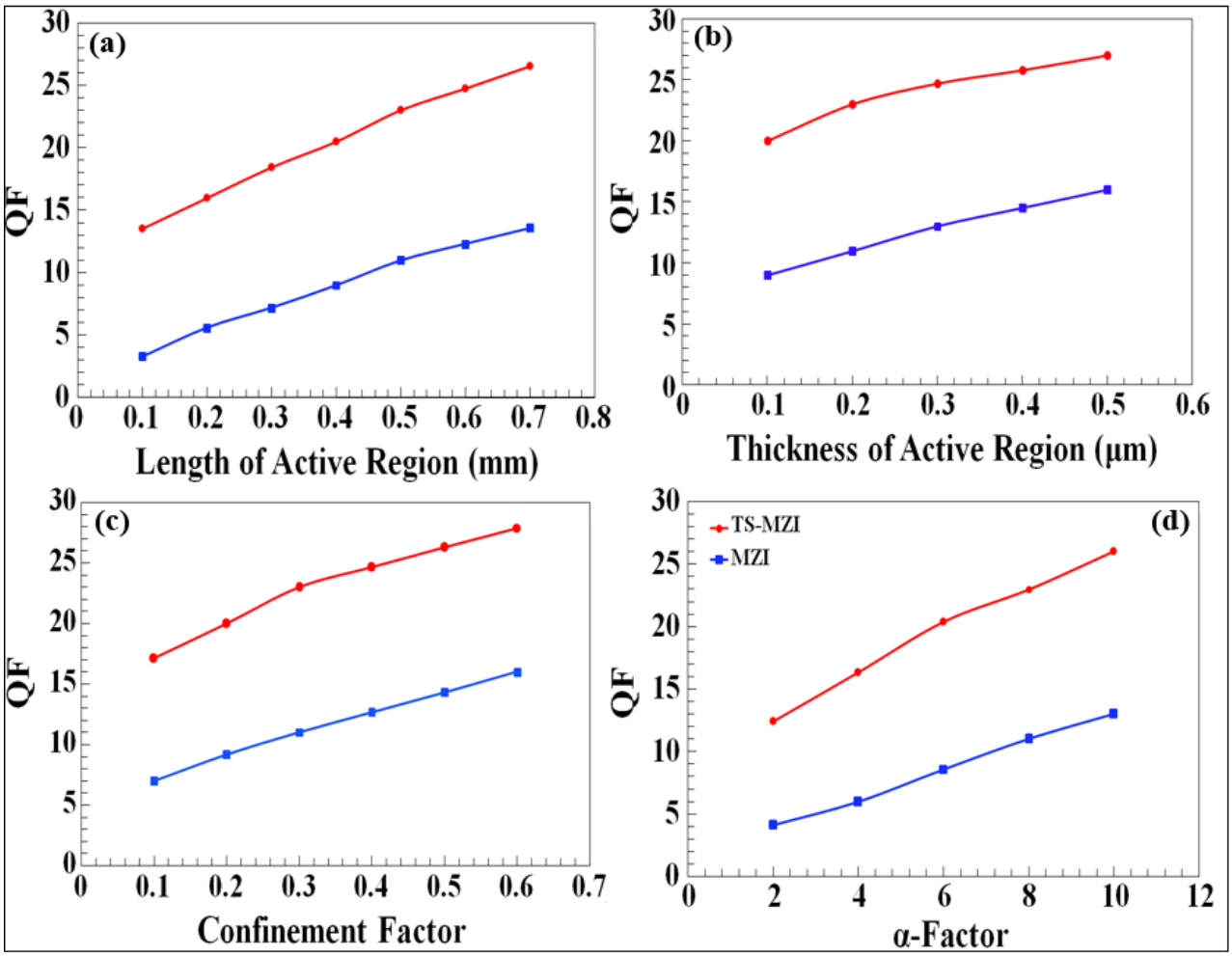

Fig. 6. QF vs. (a) length, (b) thickness of active region, (c) confinement factor, and (d) α-factor for XOR gate using SOAs-based TS-MZI and SOAs-based MZI at 160 Gb/s.

The QF dependence on the SOA injection current, saturation power, carrier lifetime, and spontaneous emission factor (N_{sp}) for the XOR operation at 160 Gb/s within the TS-MZI and MZ is shown in Fig. 7(a)-(d). The semiconductor materials would absorb the incident photons at no injection currents. The injection current is used to inject the carriers into the SOA active layer to produce the optical gain. Thus, the QF is increased with the injection current for both schemes as shown in Fig.

7(a). The similar observation is obtained in Fig. 7(b), where the QF against the saturation power, which depends on the time of the radiative recombination and the transition cross section. The saturation power increases with increasing the injection current density. On the other hand, the QF is decreased with increasing the carrier lifetime and the spontaneous emission factor as shown in Fig. 7(c) and (d), respectively. A short carrier lifetime plus the optical filters used in the TS cause a fast response of the gain and the phase of the SOA. The photons can be emitted through the amplification process due to the spontaneous emission process. These photons amplify and cause fluctuations in the amplitude and the phase of the input signals. Thus, the QF is degraded as the spontaneous emission factor increases as shown in Fig. 7(d). The impact of ASE noise has been added numerically to the XOR output power[30-33] in order to obtain realistic results.

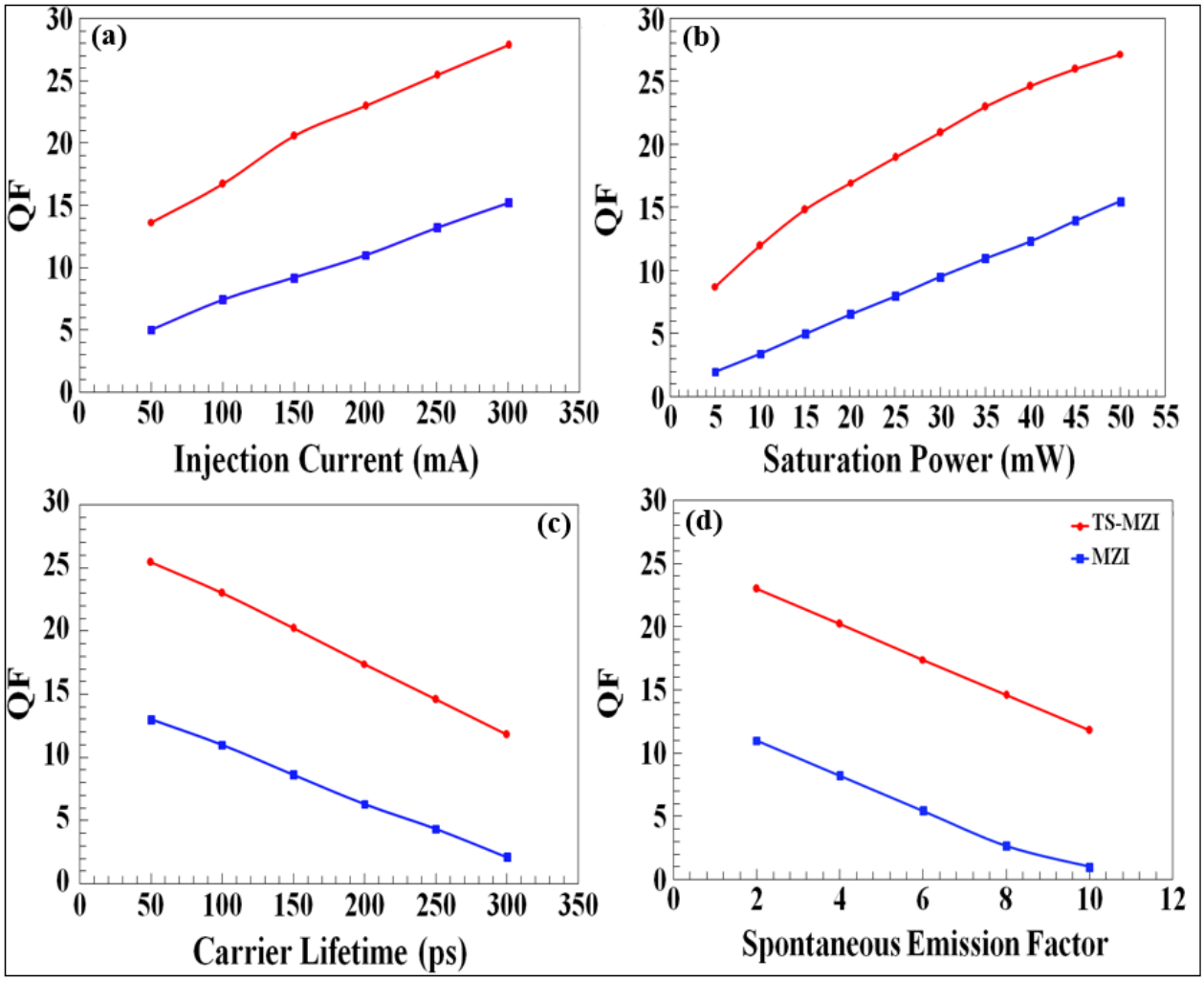

Fig. 7. QF vs. (a) injection current, (b) saturation power, (c) carrier lifetime, and (d) spontaneous emission factor for XOR gate using SOAs-based TS-MZI and SOAs-based MZI at 160 Gb/s.

4 Conclusion

In conclusion, the performance of an all-optical XOR gate using semiconductor optical amplifiers (SOAs) incorporated either in the turbo-switched (TS) or the conventional Mach-Zehnder Interferometers (MZIs) was theoretically implemented at a data rate of 160 Gb/s. The dependence of the quality factor on the key operating parameters of the input signal and SOA was investigated and assessed. The results indicate that the all-optical XOR function can be realized at 160 Gb/a with higher performance and under better-operating conditions using SOAs in the TS-MZI rather than in the standard MZI scheme.

References

[1] Kotb, "Simulation of soliton all-optical logic XOR gate with semiconductor optical amplifier," *Opt. Quantum Electron.* **48**(307), 1 (2016).

[2] Kotb and F.A. Alamer, "Dispersion on all-optical logic XOR gate using semiconductor optical amplifier," *Opt. Quantum Electron.* **48**(327), 1 (2016).

[3] P. Singh, D.K. Tripathi, S. Jaiswal, and H.K. Dixit, "Design and analysis of all-optical AND, XOR and OR gates based on SOA–MZI configuration," *Opt. Laser Technol.* **66**, 35 (2015).

[4] S. Singh, R. Kaur, and R.S. Kaler, "Photonic processing for all-optical logic gates based on Semiconductor Optical Amplifier," *Opt. Eng.* **53**, 116102 (2014).

[5] S. Singh and Lovkesh, "Ultrahigh-speed optical signal processing logic based on an SOA-MZI," *IEEE J. Sel. Top. Quantum Electron.* **18**, 970 (2012).

[6] I. Kang, M. Rasras, L. Buhl, et al., "All-optical XOR and XNOR operations at 86.4 Gb/s using a pair of semiconductor optical amplifier Mach-Zehnder interferometers," Opt. Express 17, 19062 (2009).

[7] J.M. Martínez, F. Ramos, and J. Martí, "10 Gb/s reconfigurable optical logic gate using a single hybrid-integrated SOA-MZI," *Fiber Integr. Opt.* **27**, 15 (2008).

[8] J.Y. Kim, J.M. Kang, T.Y. Kim, and S.K. Han, "10 Gbits all-optical composite logic gates with XOR, NOR, OR, and NAND functions using SOA-MZI structures," *Electron. Lett.* **42**, 303 (2006).

[9] H. Sun, Q. Wang, H. Dong, et al., "All-optical logic XOR gate at 80 Gb/s using SOA-MZI-DI," *IEEE J. Quantum Electron.* **42**, 747 (2006).

[10] Q. Wang, G. Zhu, H. Chen, et al., "Study of all-optical XOR using Mach-Zehnder Interferometer and differential scheme," *IEEE J. Quantum Electron.* **40**, 703 (2004).

[11] N.K. Dutta, Q. Wang, G. Zhu, et al., "All-Optical XOR Using Mach-Zehnder Interferometer," *Proc. ITCOM* **5595**, 269. (2004).

[12] T. Houbavlis, K.E. Zoiros, and G. Kanellos, "Design rules for implementation of 10-Gb/s all-optical Boolean XOR gate using semiconductor optical-amplifier-based Mach-Zehnder interferometer," *Opt. Eng.* **43**, 1334 (2004).

[13] T. Houbavlis, K.E. Zoiros, G. Kanellos, and C. Tsekrekos, "Performance analysis of ultrafast all-optical Boolean XOR gate using semiconductor optical amplifier-based Mach-Zehnder interferometer," *Opt. Commun.* **232**, 179 (2004).

[14] R.P. Webb, R.J. Manning, G.D. Maxwell, and A.J. Poustie, "40 Gbit/s all-optical XOR gate based on hybrid-integrated Mach-Zehnder interferometer," *Electron. Lett.* **39**, 79 (2003).

[15] M. Zhang, Y. Zhao, L. Wang, J. Wang, and P. Yea, "Design and analysis of all-optical XOR gate using SOA-based Mach–Zehnder interferometer," *Opt. Commun.* **223**, 301 (2003).

[16] H. Chen, G. Zhu, Q. Wang, J. Jaques, J. Leuthold, A.B. Piccirilli, and N.K. Dutta, "All-optical logic XOR using a differential scheme and Mach-Zehnder interferometer," *Electron. Lett.* **38**, 1271 (2002).

[17] K. Hussain, S.P. Singh, and P.K. Datta, "Effect of input signal and filter parameters on patterning effect in a semiconductor optical amplifier," *Opt. Commun.* **308**, 197 (2013).

[18] V. Nithina, Y. Kumar, and M.R. Shenoy, "Novel scheme of assist-light injection through waveguide coupling in a semiconductor optical amplifier for fast gain recovery," *Opt. Commun.* **359**, 419 (2016).

[19] Y. Kumar and M.R. Shenoy, "A Novel scheme of optical injection for fast gain recovery in semiconductor optical amplifier," *IEEE Photon. Technol. Lett.* **26**, 933 (2014).

[20] P. Tian, L. Huang, W. Hong, and D. Huang, "Pattern effect reduction in all-optical wavelength conversion using a two-electrode semiconductor optical amplifier," *Appl. Opt.* **49**, 5005 (2010).

[21] A.J. Zilkie, J. Meier, M. Mojahedi, et al., "Carrier dynamics of quantum-dot, quantum-dash, and quantum-well semiconductor optical amplifiers operating at 1.55 μm," *IEEE Quantum Electron.* **43**, 982 (2007).

[22] P. Spirito, G. Breglio, V.D'Alessandro, and N. Rinaldi, "Analytical model for thermal instability of low voltage power MOS and SOA in pulse operation," *Proc. 14th IEEE, Int. Symposium Power Semiconductor Devices and ICs* (2002).

[23] N.K. Dutta and Q. Wang, *Semiconductor Optical Amplifiers*, 2nd ed., World Scientific Publishing Company, Singapore (2013).

[24] A. Kotb, All-Optical Logic Gates Using Semiconductor Optical Amplifier, Lambert Academic Publishing, Saarbrucken (2012).

[25] A. Kotb, K.E. Zoiros, and C. Guo, "160 Gb/s photonic crystal semiconductor optical amplifiers-based all-optical logic NAND gate," *Photonic Netw. Commun.* **36**, 246 (2018).

[26] K. Komatsu, G. Hosoya, and H. Yashima, "All-optical logic NOR gate using a single quantum-dot SOA-assisted an optical filter," *Opt. Quantum Electron.* **50**, 131 (2018).

[27] D. Cassioli, S. Scotti, and A. Mecozzi, "A time-domain computer simulator of the nonlinear response of semiconductor optical amplifiers," *IEEE Quantum Electron.* **36**, 1072 (2000).

[28] A. Kotb and Y. Mohamed, "Phase-shift keying modulated data signal using SOA-MZI-based all-optical logic AND gate at 80 Gb/s," Inter. J. Opt. 2018, 5864530 (2018).

[29] R. Gutiérrez-Castrejón, "160 Gb/s XOR gate using bulk SOA turbo-switched Mach-Zehnder interferometer," *Proc. 4th Inter. Conf. on Electrical and Electron. Eng.* **4344991**, 134 (2007).

[30] A. Kotb, S. Ma, Z. Chen, N.K. Dutta, and G. Said, "Effect of amplified spontaneous emission on semiconductor optical amplifier based all-optical logic," Opt. Commun. 284, 5798 (2011).

[31] Kotb, K.E. Zoiros, and C. Guo, "All-optical XOR, NOR, and NAND logic functions with parallel semiconductor optical amplifier-based Mach-Zehnder interferometer modules," *Opt. Laser Technol.* **108**, 426 (2018).

[32] Kotb, K. E. Zoiros, and C. Guo, "Performance investigation of 120 Gb/s all-optical logic XOR gate using dual reflective semiconductor optical amplifier-based scheme," *J. Comp. Electron.* **17**, 1640 (2018).

[33] Kotb, K. E. Zoiros, and C. Guo, "Numerical investigation of all-optical logic OR gate at 80 Gb/s with dual pump-probe semiconductor optical amplifier (SOA)-assisted Mach-Zehnder interferometer (MZI)," *J. Comp. Electron.* doi: 10.1007/s10825-018-1275-9 (2018).

First author, Amer Kotb, has obtained the PhD and MSc in Electronics in 2012 and 2006, respectively. His PhD thesis is carried out at the Connecticut University in the USA. He is currently an Associate Professor of Electronics in the Guo China-US Photonics Laboratory, Changchun Institute of Optics, Fine Mechanics, and Physics, Changchun 13003, China and in the Department of Physics Faculty of Science, Fayoum University, Fayoum 63514, Egypt. He has published more than 30 international journal papers as the first author as well as one book in semiconductor optical amplifiers (SOAs)-based all-optical logic gates. He serves as an Editor and on editorial boards for a number of scientific journals. Current research activities are the investigation of: photonic crystal quantum dot (QD) SOAs, reflective SOAs, and Graphene SOAs at high data rates.

Second author, Chunlei Guo, is the director of the Guo China-US Photonics Laboratory in Changchun Institute of Optics, Fine Mechanics, and Physics, Changchun 13003, China. Prof. Guo's research interests focus on laser-matter interactions at high intensities, nano-photonics, femtosecond laser surface nano and microstructure, and surface plasmonics. He and his coworkers invented the so-called black and colored metals, which have a broad range of technological applications and have been covered extensively by the media. He is an elected Fellow for American Physical Society, Optical Society of America, and international Academy of Photonics & Laser Engineering. He serves as an Editor and on editorial boards for a number of scientific journals and is the past Chair of Short-Wavelength and High-Field Physics Group in the Optical Society of America.

